Polymeric Nanopillars Reinforced with Metallic Shells in the Lower Stem Region

Hyunsik Yoon, Moon Kyu Kwak, Sang Moon Kim, Seung Hyun Sung, Jaehoon Lim, Hyo Seon Suh, Kahp Y. Suh, and Kookheon Char**

Bioinspired polymeric high-aspect-ratio (AR) nanostructures have recently received much attention in various fields due to their unique mechanical, optical, and surface properties. In addition to microelectromechanical systems[1–3] that utilize high sensitivity, the high-AR structures were shown to be useful for dry adhesive materials,[4–8] water- or oil-repelling surfaces,[9–13] smart optical films,[14–16] nanogenerators,[17,18] and cell culture platforms for directional cell migration.[19,20] A potential limitation for widespread use in such applications is that soft high-AR structures are susceptible to mechanical instabilities, such as delamination, clumping, and clustering between neighboring features when they are used in arrayed format.[21–24] Among these, the capillary-force-induced clustering of nanopillars is the major hurdle to overcome for most practical applications because many assembled devices or systems are usually operated in water or a humid environment.[23,24]

In fact, many research groups have investigated the stability of high-AR micro- and nanopillar arrays both experimentally and theoretically.[21–24] It was noted that the pillar clustering generally takes place between two or four adjacent pillars, thereby forming a multibody assembly over a large area. Unless this clustering is intentionally or deliberately employed to realize self-assembled twisted or helical structures, as recently demonstrated by Aizenberg and coworkers,[22] such clustering is highly undesirable and detrimental to device performance and thus should be avoided by suitable surface modification.

Replica molding is a well-established method for fabricating high-AR nanostructures. Two methods can be used in this case to enhance the mechanical properties of replicated pillar or line arrays. First, the use of a rigid material directly reduces the possibility of structural collapse although it can cause a bit of difficulty in cleanly releasing the mold due to enhanced brittleness.[23] However, polymeric materials, whether they are thermoplastics or thermosets, have relatively too small a Young's modulus, typically ranging from several megapascals to gigapascals, to prevent structural collapse due to capillary forces. Second, the molded polymeric pillar array can be reinforced with the deposition of a rigid film (e.g., metal layer), effectively enhancing the mechanical property of the pillars.[25,26] Taking the latter approach, angled nanopillars 100 nm in diameter and 1 μm in height (AR = 10) have recently been employed for directional adhesion with repeating cycles of over 100 without notable collapse or reduction in adhesion strength.[26] However, direct deposition of metal on nanopillars is of limited utility in the sense that homogeneous polymer properties are sometimes totally altered by the deposited layer.

To overcome the limitations mentioned above, we developed a simple yet robust method for enhancing the mechanical properties of high-density nanopillar arrays by combining the advantages offered by oblique metal deposition[27–30] following replica molding.[31] Herein, we present a method for fabricating such a nanopillar array structure, the stem region of which is coated with a metal layer and thus strengthened, with the top part of the pillar intact and soft. We demonstrate that the reinforced nanostructures show remarkable stability against structure collapse by capillary-force-induced clustering. In addition, with a theoretical approach, we provide a model to predict the conditions (metal coverage and metal layer thickness) to avoid clustering. Also, the top surface of the nanopillars can be utilized for making hollow structures or decorated with materials of special functions, because the top part of the pillar is not covered by metal film.

The procedure for fabricating the reinforced nanostructures is shown schematically in **Figure 1**. After surface treatment with a fluorinated self-assembled monolayer (SAM) for easy release from the master, a gold film was deposited obliquely at an angle onto the master that had been produced by a conventional photolithography and dry etching process. The same step was repeated after 180° rotation. The purpose of the two-step deposition is just for symmetry. Therefore, we can omit the second step of deposition or change the metal coverage by adjusting the oblique angle during

Dr. H. Yoon, S. H. Sung, J. Lim, H. S. Suh, Prof. K. Char
The National Creative Research Initiative Center for Intelligent Hybrids
School of Chemical and Biological Engineering
The WCU Program of Chemical Convergence for Energy and Environment
Seoul National University
Seoul 151-744, Korea
E-mail: khchar@plaza.snu.ac.kr
Dr. M. K. Kwak, S. M. Kim, Prof. K. Y. Suh
School of Mechanical and Aerospace Engineering
The WCU Program on Multiscale Mechanical Design
Seoul National University
Seoul 151-744, Korea
E-mail: sky4u@snu.ac.kr

DOI: 10.1002/smll.201101114

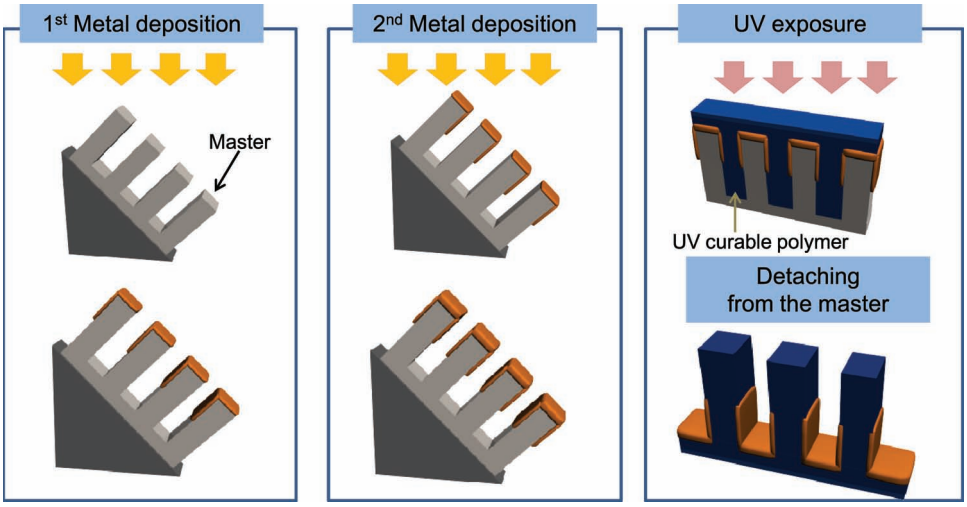

Figure 1. Schematic illustration of the fabrication of polymeric nanopillars reinforced with metal shells in the lower stem region. After surface treatment of a master for easy detachment, a metal film is obliquely deposited on the master. For symmetry of metal shells around polymer nanopillars, the master is rotated 180° and a second deposition is performed after the first oblique deposition. Subsequently, a UV-curable PUA precursor is backfilled into the master mold and cured by UV exposure. The polymer nanopillars reinforced with metal shells in the lower stem region are finally detached from the master.

deposition. Then, a precursor of UV-curable polyurethane acrylate[32] (PUA, Young's modulus: 20 MPa) was drop-dispensed, pressed by a polyethylene terephthalate (PET) backing layer, and detached from the master after UV curing, thus leaving behind composite PUA nanostructures with the lower region coated by a metallic shell. As discussed in our previous report[31] about the metal transfer, the detachment of metal films from the silicon master results from the difference of adhesive force between the polymer/metal- and metal/SAM-treated silicon master. Here, the SAM treatment turned out be critical in the subsequent transfer of Au film to the polymer structure; otherwise, the metal transfer was not reproducible and frequently yielded a nonuniformly distributed metal shell. With the help of the surface modification, the transfer was almost complete over 100 times of replication for the PUA currently used in our experiments and other UV-curable resins such as Norland optical adhesive (NOA). The method is also applicable to thermoplastic polymers such as polystyrene (PS). In this case, we raised the processing temperature to melt the thermoplastic polymer, and then we filled the melt into the master. After cooling, we detached the solidified polymer from the master. In contrast, the transfer was not successful in the case of elastomeric polydimethylsiloxane (PDMS), which is known for its inert and low adhesion to most surfaces. Large-area views of silicon masters (before and after the oblique metal deposition) and PUA backfilling for replication are shown in Figure S1 (Supporting Information).

To evaluate the resistance against capillary-force-induced collapse due to contact with water, we dipped the prepared reinforced structure of nanopillars into water for 30 min, followed by drying in ambient air. **Figure 2** shows the test results under two different conditions: 1) changing metal thickness at a constant oblique deposition angle of 22° (a–c) and 2) varying metal coverage with a constant metal thickness of 80 nm (d–f). Scocanning electron microscopy (SEM) images of the patterns were obtained using a Philips XL30FEG microscope. To avoid charging effects, the polymeric nanopillars were sputter-coated 5 nm thick with Pt prior to measurements. The

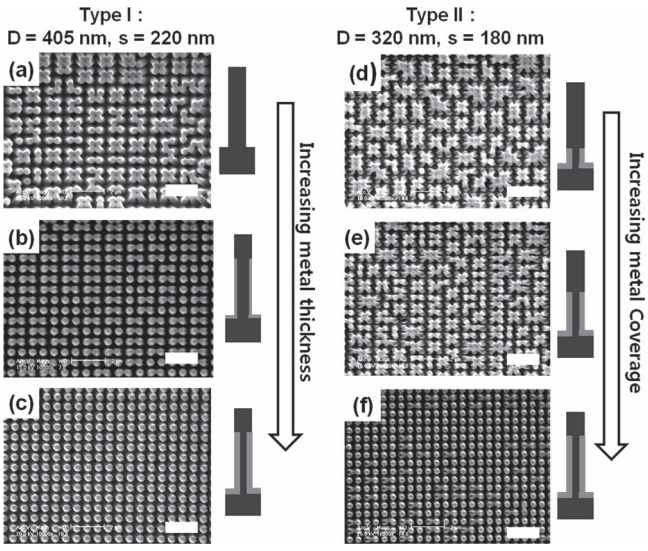

Figure 2. SEM images showing the enhanced stability of polymeric nanopillars fortified with metal shells in the lower stem region against capillary force, which typically induces clustering of polymer nanopillars. a–c) Samples with increasing metal film thickness at a fixed oblique angle of 22° (0, 40, and 80 nm metal film thickness for the first, second, and third frames in the first column, respectively). d–f) Samples with increasing metal coverage with a fixed metal thickness of 80 nm (the metal coverage fraction is 0.22, 0.39, and 0.79 for the first, second, and third frames in the second column, respectively). Polymeric nanopillar dimensions are: Type I, 405 nm in diameter (*D*), 220 nm center-to-center distance (*s*), and 1 μm in height (with AR ≈ 2.5); Type II, 320 nm diameter (*D*), 180 nm center-to-center distance (*s*), and 1 μm height (with AR ≈ 3.1). The scale bar in the SEM images is 2 μm.

small NANO MICRO

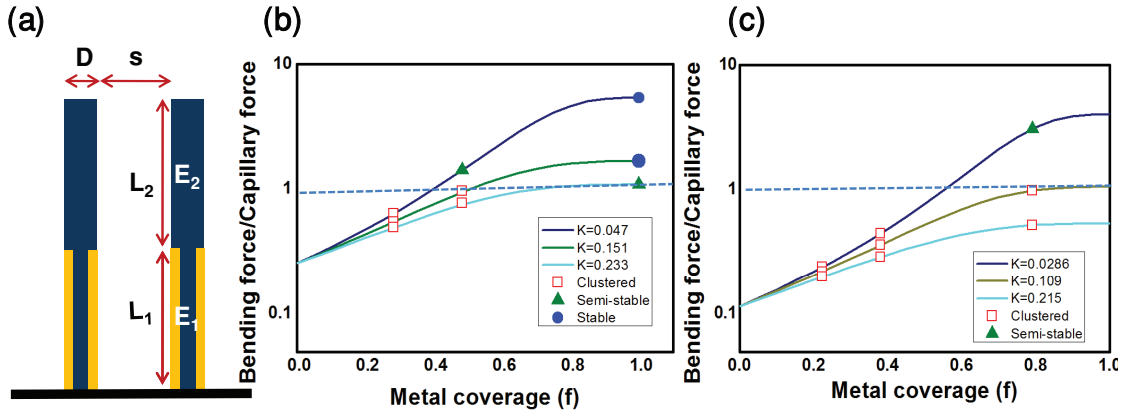

Figure 3. a) Schematic of the metal-reinforced polymer nanopillars with two different moduli in the vertical direction. b) Comparison of F_E/F_c derived from Equations (4) and (6) with experimental data for the Type I nanopillars. The open squares, filled triangles, and filled circles indicate collapsed, partially collapsed, and stable nanopillars, respectively. c) Comparison between theoretical predictions and experimental data for the Type II nanopillars. It is noted that the theoretical predictions are all in good agreement with the experimental data.

metal coverage, or the fraction of the pillar surface covered with metal, was varied as a function of the oblique deposition angle, as described in Figure S2 (Supporting Information). Two different types of nanopillars were employed: 405 nm in diameter, 220 nm spacing between pillars, and 1 μm in height (Type I, first column in Figure 2, with AR ≈ 2.5); and 320 nm in diameter, 180 nm spacing, and 1 μm in height (Type II, second column in Figure 2, with AR ≈ 3.1). As is apparent from Figure 2a–c, the degree of pillar clustering decreases with increasing metal thickness (0, 40, and 80 nm in the first, second, and third frames, respectively, in the first column). In particular, there was virtually no observable pillar clustering over a large area for the Type I nanopillars when the metal thickness was 80 nm, which suggests that the nanopillars were sufficiently reinforced to overcome the collapse of polymeric pillars by the capillary force.

The oblique deposition angle (θ_{in}) was varied to obtain various metal coverages at a fixed metal film thickness of 80 nm (0.22, 0.39, and 0.79 in the first, second, and third frames in the second column, respectively). As shown in Figure 2e and f, the pillar clustering was significantly reduced at high metal coverages (or smaller θ_{in}). Despite the relatively high metal film thickness of 80 nm, the polymeric nanopillars collapsed at the intermediate metal coverage of 0.22 for Type II nanopillars, thus implying that the metal coverage is the dominant factor in preventing the structure collapse by capillary-force-induced condensation. The cross-sectional SEM images are shown in Figure S3 (Supporting Information).

The mechanical stability of the reinforced nanopillars with metallic shells in the lower stem region can be investigated in terms of the competition between the elastic restoring force (stabilizing) and the capillary force between neighboring nanopillars (destabilizing). **Figure 3**a shows a schematic of the composite bilayered nanopillars with different moduli in the vertical direction. The Young's modulus of the soft, polymeric top region (E_2) would be much smaller than that of the metal-supported bottom region (E_1), the ratio of which is determined by the metal film thickness. Referring to the definition used in Figure S4 (Supporting Information), the governing equation for the deflection of a beam can be written as:[33]

$$E I \frac{d^2 v}{dx^2} = M \tag{1}$$

where E is the Young's modulus of the pillar, I is the moment of inertia, v is the deflection, and M is the bending moment. The bending moment at a distance x from the fixed support is obtained from the free-body diagram of Figure 3a. Note that the vertical reaction at the support is equal to F and the moment reaction is equal to $(L_1 + L_2)F$. Consequently, the expressions for M are:

$$M = -F(L_1 + L_2) + Fx \rightarrow (0 < x < L_1) \tag{2}$$

$$M = -F(L_1 + L_2 - x) \rightarrow (L_1 < x < L_2) \tag{3}$$

Solving the above second-order differential equation with suitable initial and boundary conditions leads to the following expression for the elastic restoring force F_E (a detailed derivation is provided in the Supporting Information, Figure S4):

$$F_E = \frac{s E_1 D^4}{4L^3} / \left(1 + (1-f)^3\right) \left(\frac{1}{K} - 1\right) \tag{4}$$

where s is the distance between two adjacent nanopillars before bending, D is the diameter of the nanopillar, f is the coverage ratio [$= L_1/(L_1+L_2)$], and K is the modulus ratio ($K = E_2/E_1$). Here, the effective modulus E_1 of the metal-covered stem region is given in the literature [Eq. (5)]:[34]

$$E_1 = \frac{E_m^2 \left(\frac{t_m}{t}\right)^4 + E_p^2 \left(\frac{t_p}{t}\right)^4 + 2 E_m E_p \frac{t_m}{t} \frac{t_p}{t} \left[2 \left(\frac{t_m}{t}\right)^2 + 2 \left(\frac{t_p}{t}\right)^2 + 3 \frac{t_m}{t} \frac{t_p}{t}\right]}{E_m \frac{t_m}{t} + E_p \frac{t_p}{t}} \tag{5}$$

where E_m is the metal modulus (≈79 GPa for Au), E_p is the modulus of PUA (≈20 MPa), t_m is the thickness of the metal film, and t_p is the thickness of the PUA pillar.

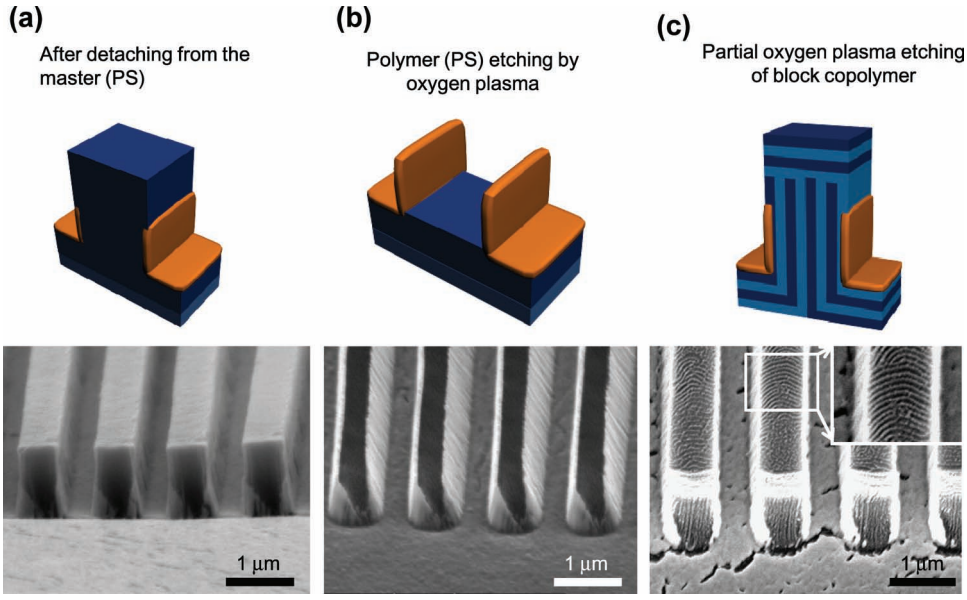

Figure 4. a) SEM image showing PS line patterns (600 nm in width and 1 μm in height) coated by Au shell films in the lower wall region. The metal coverage is about 0.6. b) SEM image showing thin gold nanowall films (40 nm in width and 600 nm in height, AR = 15) after removing the PS pillars by oxygen plasma etching. c) SEM image of a diblock copolymer pattern reinforced by metallic shell in the lower stem region after partial oxygen plasma etching to reveal a self-assembled pattern. The typical fingerprint pattern is revealed after removing the top surface of the block copolymer.

The destabilizing capillary force F_c can be derived as a function of pillar geometry and water surface tension. If the meniscus is formed at the upper part of the structure, the capillary force between two neighboring pillars partially immersed in a liquid is derived as [Eq. (6)]:[23]

$$F_c = \frac{\pi \gamma D^2 \cos^2 \theta}{2\sqrt{(D+\delta)^2 - D^2}} \quad (6)$$

where D is the pillar diameter, γ is the surface tension of liquid (water = 0.073 N m^{-1}), θ is the contact angle between liquid and pillar surface, and δ is the distance between the pillars after bending by the capillary force. The capillary-force-induced pillar collapse will not take place if the elastic bending force is larger than the capillary force existing between nanopillars. For a specific example, we calculated the capillary force with the assumptions that $\theta = 60°$ and the distance δ between the pillars after bending is 2 nm.

Figure 3b and c show a comparison between experimental data (b: Type I and c: Type II) and theoretical predictions of F_E/F_c derived from Equations (4) and (6). The open squares, filled triangles, and filled circles indicate the collapsed, partially collapsed (semi-stable in Figure 3), and stable nanopillars, respectively. When F_E/F_c is larger than unity, the elastic bending force is higher than the capillary force, thereby preventing the structural pillar collapse. When F_E/F_c is less than unity, on the other hand, the pillars collapse due to the dominant capillary force. In both cases, the theoretical predictions are in good agreement with the experimental data.

One unique advantage of the stem-reinforced structure presented here is that the top surface of the high-AR nanostructure can be exploited for various applications. Also, the method is versatile in materials used because we can employ thermoplastic polymers as well. **Figure 4**a shows such an example where PS lines (600 nm in width and 1 μm in height) were employed as a sacrificial layer for dry etching. After selective oxygen plasma etching of polymer, hollow structures with high-AR metallic nanowalls (40 nm in width and 600 nm in height, AR = 15) are produced along the polymeric lower stem region (Figure 4b). One can also utilize a special polymer such as block copolymers or other hybrid materials. Figure 4c shows the SEM image of the PS-*b*-poly(methyl methacrylate) (PMMA) diblock copolymer line pattern (700 nm in width and 1 μm in height) covered by a metallic shell in the lower stem region after partial oxygen plasma etching, to reveal self-assembled patterns by exploiting the difference in etching rates of PS and PMMA. The typical fingerprint patterns are shown after removing the top surface of the block copolymer. We note that when nanopillars are fabricated instead of line patterns, the metal coverage is not uniform along the vertical direction, as evidenced in the Supporting Information (Figure S5). We believe this nonuniformity is due to the substrate not being continuously rotated during the oblique metal deposition process.

To further demonstrate the usefulness of the nanostructures covered by metallic shell only in the lower stem region, we deposited green-fluorescent $Cd_{1-x}Zn_xSe_{1-y}S_y$ nanocrystals (quantum dots, QDs)[35] on the polymer side of the nanopillars. In this way, one could endow the top polymeric surface with special functions, with fluorescent dyes or semiconductor nanocrystals. As shown in **Figure 5**a, after two oblique metal depositions on a silicon master, a QD solution in toluene was spin-coated onto the master mold and a PUA replica was then prepared by the same procedure as that described earlier. The resulting PUA nanopillars possess QDs on the polymer side, which is well demonstrated by the fluorescence

small NANO MICRO

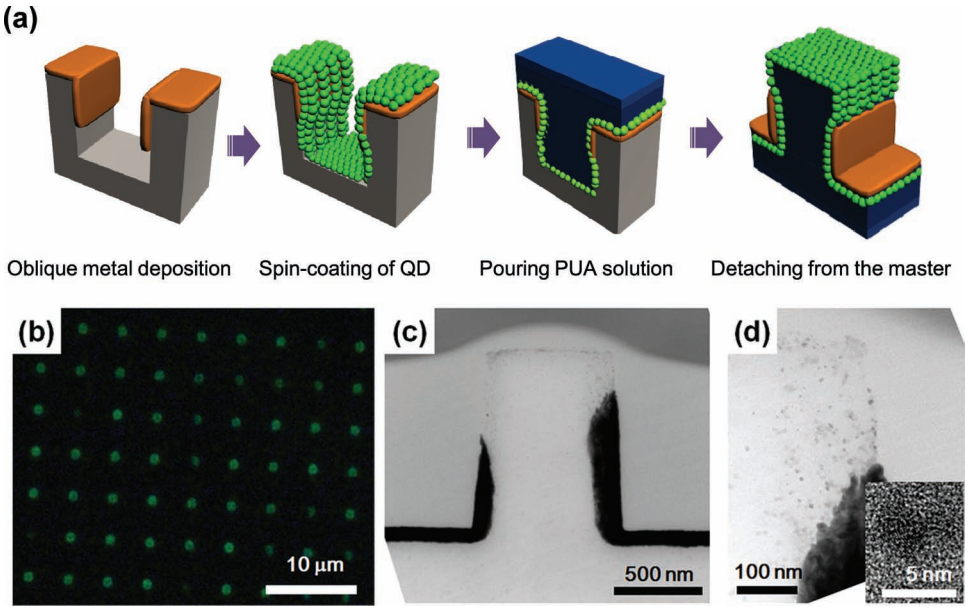

Figure 5. a) Schematic illustration showing stemmed polymer nanopillars with semiconductor nanocrystals (QDs) covering the pillar surface. After oblique metal deposition, QDs dissolved in toluene (1 wt%) were spin-coated on the metal-deposited master. PUA precursor was then poured into the master mold, cured by UV exposure, and the molded sample was detached from the master. b) Fluorescence microscopic image showing the green emission from $Cd_{1-x}Zn_xSe_{1-y}S_y$ nanocrystals (QDs) residing on the top surface of polymeric nanopillars. c) TEM image showing metallic shells at the lower stem region as well as at the top surface covered by QDs. The asymmetric feature of deposited metal shells originates from the nonuniform height distribution on nanopillars, as illustrated in Figure S4. d) Magnified image of (c) near the boundary between a metal shell and a bare polymer pillar. Inset: high-resolution TEM image showing the lattice structure of $Cd_{1-x}Zn_xSe_{1-y}S_y$ nanocrystals employed in the present experiment.

image shown in Figure 5b. The distribution of QDs within the polymeric pillar was also verified by transmission electron microscopy (TEM, JEOL JSM-890 at 200 kV; see Figure 5c and d). The TEM images show metallic shells at the lower stem region as well as at the top surface covered by QDs. The asymmetric feature of the deposited metal shells originates from the nonuniform height distribution on nanopillars, as illustrated in Figure S5 (Supporting Information).

In summary, we have devised and fabricated a reinforced polymeric nanostructure with metallic shells in the lower stem region. The stem part of the pillar is made mechanically stiff and strong by surrounding it with metal, while the top part of the pillar is intact and soft. The simple yet robust fabrication method was shown to be predictable with the theoretical development made here, which compares well with experimental results. The fact that the top part of the pillars is not covered by a metallic shell could be used for fabricating hollow structures with high-AR metallic nanowalls, and for decorating the top of the nanopillars with functional materials such as QDs. This mechanical reinforcement with deposited metal films only in the lower stem region and the possibility to decorate or utilize the uncovered top parts of the pillars enables applications in humid or water environments.

Experimental Section

The silicon master was prepared by photolithography followed by reactive-ion etching. The master was treated with a fluorinated SAM solution ((tridecafluoro-1,1,2,2-tetrahydrooctyl)-trichlorosilane: FOTCS, Gelest Corp.) that had been diluted to 0.03 M with anhydrous heptane (Samchon Corp.) in an Ar environment. The treated master mold was annealed at 120 °C for 20 min. We coated the master with a metal film (Au) by oblique metal deposition (200 Å min^{-1}) with varying thickness and oblique angle. A thermal evaporator was used for metal deposition, in which the master was placed on an inclined holder as described in our previous report.[27] The vacuum condition for the metal deposition was 10^{-6} Torr. During the deposition process, evaporated metal atoms were guided down vertically, but the inclined holder caused the oblique incidence angle, thereby leading to metal layers deposited only on one side of the master. To guarantee the symmetry, the metal-deposited master was rotated 180° following the first oblique metal deposition. Then drops of soft PUA (301RM, Minuta Tech) prepolymer were dispensed onto the master and a flexible PET film (≈50 μm) was slightly pressed against the liquid drop to be used as a supporting backing layer. After preparing a polymer replica by UV exposure, the PUA replica was removed from the mold. Details of the synthesis and characterization of the PUA can be found elsewhere.[32] To demonstrate the possibility of using a thermoplastic polymer, we purchased commercial PS (MW = 100 000, Aldrich) and prepared a 10 wt% solution in toluene. The PS film was coated onto the PET substrate that had been treated with an adhesion promoter. The PS-coated PET film was subsequently placed on the Au-deposited silicon master. Then, the temperature was raised to ≈160 °C to fill up the PS melt under pressure (≈4 bar) and the PS replica was removed after cooling to room temperature. With the help of the difference in adhesion forces, the metal film (≈40 nm in thickness) was transferred to the lower stem region of the PS structures. A diblock copolymer (129.5 kg mol^{-1}

(66k–63.5k), PS-*b*-PMMA, Polymer Source Inc.) was also used as another thermoplastic polymer to demonstrate the fabrication of complex structures. The procedure was the same as with PS, and the molding temperature was 220 °C for 20 min. PS-*b*-PMMA film was prepared by drop-casting of a 1 wt% solution of PS-*b*-PMMA in toluene on a PET substrate.

High-resolution SEM images of the patterns were obtained using a Philips XL30FEG instrument. To avoid charging effects, the polymeric nanopillars were sputter-coated 5 nm thick with Pt prior to measurements. TEM images were obtained using a JEOL JSM-890 microscope at 200 kV.

Supporting Information

Supporting Information is available from the Wiley Online Library or from the author.

Acknowledgements

This work was supported by the National Creative Research Initiative Center for Intelligent Hybrids (No. 2010-0018290) through National Research Foundation of Korea (NRF) grants, the World Class University (WCU) Programs (R31-10013, R31-2008-000-10083-0), an NRF grant (No. 20110017530), and the Brain Korea 21 Program funded by the Ministry of Education, Science, and Technology (MEST).

[1] a) M. E. McConney, K. D. Anderson, L. L. Brott, R. R. Naik, V. V. Tsukruk, *Adv. Funct. Mater.* **2009**, *19*, 2527; b) M. J. McHenry, J. A. Stother, S. M. Van Netten, *J. Comp. Physiol. A* **2008**, *194*, 795.
[2] B. Pokroy, A. K. Epstein, M. C. M. Persson-Gulda, J. Aizenberg, *Adv. Mater.* **2009**, *21*, 463.
[3] B. A. Evans, A. R. Shields, R. L. Carroll, S. Washburn, M. R. Falvo, R. R. Superfine, *Nano Lett.* **2007**, *7*, 1428.
[4] K. Autumn, Y. A. Liang, S. T. Hsieh, W. Zesch, W. P. Chan, T. W. Kenny, R. Fearing, R. J. Full, *Nature* **2000**, *405*, 681.
[5] A. K. Geim, S. V. Dubonos, I. V. Grigorieva, K. S. Novoselov, A. A. Zhukov, S. Y. Shapoval, *Nat. Mater.* **2003**, *2*, 461.
[6] A. del Campo, E. Arzt, *Chem. Rev.* **2008**, *108*, 911.
[7] H. Yoon, H. E. Jeong, T. I. Kim, T. J. Kang, D. Tahk, K. Char, K. Y. Suh, *Nano Today* **2009**, *4*, 385.
[8] J. H. Lee, R. S. Fearing, K. Komvopoulos, *Appl. Phys. Lett.* **2008**, *93*, 191910.
[9] R. Blossey, *Nat. Mater.* **2003**, *2*, 457.
[10] K. K. S. Lau, J. Bico, K. B. K. Teo, M. Chhowalla, G. A. J. Amaratunga, W. I. Milne, G. H. Mckinley, K. K. Gleason, *Nano Lett.* **2003**, *3*, 1701.
[11] T. Sun, L. Feng, X. Gao, L. Jiang, *Acc. Chem. Res.* **2005**, *38*, 644.
[12] J. Shieh, F. J. Hou, Y. C. Chen, H. M. Chen, S. P. Yang, C. C. Cheng, H. L. Chen, *Adv. Mater.* **2010**, *22*, 597.
[13] F. Xia, L. Jiang, *Adv. Mater.* **2008**, *20*, 2842.
[14] P. Vukusic, J. R. Sambles, *Nature* **2003**, *424*, 852.
[15] S. Kinoshita, S. Yoshioka, J. Miyazaki, *Rep. Prog. Phys.* **2008**, *71*, 076401.
[16] A. R. Parker, H. E. Townley, *Nat. Nanotechnol.* **2007**, *2*, 347.
[17] Z. L. Wang, J. Song, *Science* **2006**, *312*, 242.
[18] M. P. Lu, J. Song, M. Y. Lu, M. T. Chen, Y. Gao, L. J. Chen, Z. L. Wang, *Nano Lett.* **2009**, *9*, 1223.
[19] D. H. Kim, P. K. Wong, J. Park, A. Levchenko, Y. Sun, *Annu. Rev. Biomed. Eng.* **2009**, *11*, 203.
[20] D. H. Kim, C. H. Seo, K. Han, K. W. Kwon, A. Levchenko, K. Y. Suh, *Adv. Funct. Mater.* **2009**, *19*, 1579.
[21] H. Duan, K. K. Berggren, *Nano Lett.* **2010**, *10*, 3710.
[22] B. Pokroy, S. H. Kang, L. Mahadevan, J. Aizenberg, *Science* **2009**, *323*, 237.
[23] D. Chandra, S. Yang, *Langmuir* **2009**, *25*, 10430.
[24] D. Chandra, S. Yang, *Acc. Chem. Res.* **2010**, *43*, 1080.
[25] K. Y. Suh, R. Langer, J. Lahann, *Appl. Phys. Lett.* **2003**, *83*, 4250.
[26] T. I. Kim, H. E. Jeong, K. Y. Suh, H. H. Lee, *Adv. Mater.* **2009**, *21*, 2276.
[27] H. Yoon, H. Woo, M. K. Choi, K. Y. Suh, K. Char, *Langmuir* **2010**, *26*, 9198.
[28] N. Li, S. R. Forrest, *Appl. Phys. Lett.* **2009**, *95*, 123309.
[29] Y. Choi, S. Hong, L. P. Lee, *Nano Lett.* **2009**, *9*, 3726.
[30] K. H. Chu, R. Xiao, E. N. Wang, *Nat. Mater.* **2010**, *9*, 413.
[31] M. K. Kwak, T. I. Kim, P. Kim, H. H. Lee, K. Y. Suh, *Small* **2009**, *8*, 928.
[32] S. Choi, P. J. Yoo, S. J. Beak, T. W. Kim, H. H. Lee, *J. Am. Chem. Soc.* **2004**, *126*, 7744.
[33] J. M. Gere, S. P. Timoshenko, *Mechanics of Materials*, PWS Publishing Company, Boston, **1997**.
[34] D. Ramos, J. Mertens, M. Calleja, J. Tamayo, *Sensors* **2007**, *7*, 1757.
[35] W. K. Bae, K. Char, H. Hur, S. Lee, *Chem. Mater.* **2008**, *20*, 531.

Received: June 5, 2011
Published online: September 5, 2011